Geophysical Research Letters

RESEARCH LETTER
10.1029/2018GL081092

Influence of Atmospheric Transport on Estimates of Variability in the Global Methane Burden

Sudhanshu Pandey[1,2], Sander Houweling[1,3], Maarten Krol[2,4], Ilse Aben[1], Narcisa Nechita-Banda[2], Kirk Thoning[5], Thomas Röckmann[2], Yi Yin[6], Arjo Segers[7], and Edward J. Dlugokencky[5]

[1]SRON Netherlands Institute for Space Research, Utrecht, Netherlands, [2]Institute for Marine and Atmospheric Research Utrecht, Utrecht University, Utrecht, Netherlands, [3]Department of Earth Sciences, Vrije Universiteit Amsterdam, Amsterdam, Netherlands, [4]Meteorology and Air Quality, Wageningen University & Research, Wageningen, Netherlands, [5]Global Monitoring Division, NOAA Earth System Research Laboratory, Boulder, CO, USA, [6]Division of Geological and Planetary Sciences, California Institute of Technology, Pasadena, CA, USA, [7]Department of Climate, Air and Sustainability, TNO, Utrecht, Netherlands

Abstract We quantify the impact of atmospheric transport and limited marine boundary layer sampling on changes in global and regional methane burdens estimate using tracer transport model simulations with annually repeating methane emissions and sinks but varying atmospheric transport patterns. We find the 1σ error due to this transport and sampling effect on annual global methane increases to be 1.11 ppb/year and on zonal growth rates to be 3.8 ppb/year, indicating that it becomes more critical at smaller spatiotemporal scales. We also find that the trends in inter-hemispheric and inter-polar difference of methane are significantly influenced by the effect. Contrary to a negligible trend in the inter-hemispheric difference of measurements, we find, after adjusting for the transport and sampling, a trend of 0.37 ± 0.06 ppb/year. This is consistent with the emission trend from a 3-D inversion of the measurements, suggesting a faster increase in emissions in the Northern Hemisphere than in the Southern Hemisphere.

Plain Language Summary Changes in global and regional atmospheric burdens of methane are determined by the net effect of sources and sinks and atmospheric transport. Many studies approximate the burdens based on measurements from a network of globally distributed surface air sampling sites. Here we quantify the impact of atmospheric transport and limited marine boundary layer sampling (transport and sampling) on changes in global and regional methane burden estimates using tracer transport model simulation with annually repeating methane emissions and sinks but varying atmospheric transport patterns. We find that for assessing the annual global methane increases, a measurement-only approach is fairly accurate. However, extending the measurement-only analysis to hemispheric or latitudinal variations is more problematic as transport influences quickly become significant or even dominant. We find a large impact of transport and sampling effect on the inter-hemispheric and inter-polar difference.

Key Points:
- Transport gives rise to CH_4 variations in the spatiotemporal gradients, which are not caused by source or sink changes
- We find the transport and sampling error on annual global CH_4 increases to be 1.11 ppb/year and on zonal growth rates to be 3.8 ppb/year
- The transport-adjusted inter-hemispheric difference has a trend of 0.37 ppb/year, consistent with the emission trend from a 3-D inversion

Supporting Information:
- Supporting Information S1

Correspondence to:
S. Pandey,
s.pandey@uu.nl

Citation:
Pandey, S., Houweling, S., Krol, M., Aben, I., Nechita-Banda, N., Thoning, K., et al. (2019). Influence of atmospheric transport on estimates of variability in the global methane burden. *Geophysical Research Letters*, *46*, 2302–2311. https://doi.org/10.1029/2018GL081092

Received 30 OCT 2018
Accepted 20 JAN 2019
Accepted article online 29 JAN 2019
Published online 25 FEB 2019

1. Introduction

The atmospheric methane (CH_4) growth rate shows significant interannual variability, which is poorly understood and is heavily debated in the scientific community (Dlugokencky et al., 2011; Hausmann et al., 2016; Kirschke et al., 2013; Rigby et al., 2017; Schaefer et al., 2016; Schwietzke et al., 2016; Turner et al., 2017; Worden et al., 2017). Several studies analyzing the CH_4 growth rate variations make use of marine boundary layer (MBL) measurements in combination with simple box models (Nisbet et al., 2016; Rigby et al., 2017; Turner et al., 2017; Worden et al., 2017). The implicit assumption made in these studies is that averages of the available measurement sites in the MBL are representative of the global, hemispheric, or zonal burden of atmospheric CH_4.

The regional and global burdens (the global burden is the burden of the whole atmosphere) of CH_4 are determined by surface emissions and atmospheric sinks—mainly by reaction with oxidants like OH, Cl, and $O(^1D)$—and by atmospheric transport. While the direct effect of atmospheric transport cancels in the global burden estimate, it still influences the global burden as it determines the distribution of CH_4 in the atmosphere (Warwick et al., 2002). The sink of CH_4 depends on the oxidant concentrations to which CH_4 is

exposed. As the concentration of these oxidants varies strongly, for example, from the poles to the tropics, the global sink is influenced by transport.

The transport influence on the CH_4 burden estimate can increase substantially when the burden is approximated using measurements from a limited number of MBL sites. Transport can alter growth rates over annual time scales by varying convective activity, prevailing winds, and transport times from source regions to measurement sites (Chen & Prinn, 2005).

While the influence of changing sources and sinks of CH_4 on the observed interannual variability has been discussed in several studies (Hausmann et al., 2016; Rigby et al., 2017; Schaefer et al., 2016; Schwietzke et al., 2016; Turner et al., 2017; Worden et al., 2017), the role of atmospheric transport has received only limited attention. While Warwick et al. (2002) and Chen and Prinn (2005) addressed the atmospheric transport, their focus was on the signals observed at individual sites and they analyzed time periods before the recent renewed increase in the CH_4 growth rate: 1980 to 1998 for Warwick et al. (2002) and 1996 to 2001 for Chen and Prinn (2005).

The U.S. National Oceanic and Atmospheric Administration Earth System Research Laboratory's Global Monitoring Division (referred to as NOAA from here on) regularly monitors CH_4 (and other climate-related tracers) from a globally distributed network of air sampling sites (see, e.g., Dlugokencky et al., 2017, 1994). The assessment of the global CH_4 burden derived by NOAA based on these measurements involves a careful assessment of the representativeness of different stations. Only a subset of network sites that sample well-mixed MBL air representative of large geographical regions is used to calculate global and zonal surface means. The use of MBL data is attractive because estimates of the global trend are obtained, based only on measurements (i.e., without using atmospheric transport models; see Dlugokencky et al., 1994). To derive an estimate of the global and regional burdens—and their trends—from a limited number of MBL sites, NOAA measurements undergo a curve fitting and data extension method as described in Masarie and Tans (1995). This method is referred to here as the "NOAA method."

Using the NOAA method, globally averaged surface CH_4 (monthly and annual means) and annual global CH_4 increases are reported at www.esrl.noaa.gov/gmd/ccgg/trends_ch4/. Besides the annual increases, the NOAA method also provides zonal growth rates per latitude band. Three-dimensional contour plots of CH_4 zonal growth rates, as a function of time and latitude, have been used in some studies to identify the likely geographical origin of large CH_4 growth rate anomalies (Nisbet et al., 2014, 2016). For example, Nisbet et al. (2014) suggested that the renewed increase in CH_4 growth rate in 2007 started in the northern extra tropics, most likely the Arctic region.

Further, spatial gradients are also derived from the NOAA method. The inter-hemispheric difference (IHD) in CH_4 abundance has been used to quantify the ratio between Northern and Southern Hemisphere CH_4 emissions or sinks. This constraint is implicitly used in two-box model studies (Rigby et al., 2017; Sapart et al., 2012., Turner et al., 2017) and multiple-box model studies (Nisbet et al., 2016; Thompson et al., 2018). Dlugokencky et al. (2003) furthermore introduced the metric inter-polar difference (IPD) as the difference between the annual averages of CH_4 from northern (53°N to 90°N) and southern (53°S to 90°S) polar regions, weighted with the inverse sine of latitude.

Since MBL measurements are sparse and are not sensitive to upper layers of the atmosphere, the question arises how well these stations observe the global and regional CH_4 burden gradients. The next section describes our approach to address this question, which is followed by a *results* section. The results are followed by a *discussion and conclusions* section, highlighting the implications of our findings.

2. Method

We address the question of representativeness of MBL measurements of CH_4 burden gradients using the atmospheric tracer transport model TM5 (Krol et al., 2005). To isolate the influence of variations in atmospheric transport, TM5 simulations for the period 1990–2016 are performed with annually repeating CH_4 sources and sinks but varying transport based on ECMWF ERA-Interim meteorological data (Dee et al., 2011). The temperature fields of 2008 were also repeated annually, to avoid interannual variations in the chemical lifetime of CH_4 due to the influence of temperature on chemical reaction rates. Section S1 in the

supporting information describes the setup of the TM5 model simulation in detail. In this study, we focus on the representativeness of NOAA's MBL measurements and analysis method. Annual global CH_4 increases, zonal growth rates, and spatial gradients, like IHD and IPD, are derived by sampling TM5 at NOAA's MBL sites and applying the same site selection, filtering, and interpolation method as applied by NOAA to the model-sampled observations. This NOAA method is briefly described in section S2. We also calculate the time series gradients in global and hemispheric atmospheric burden in the TM5 model (see section S3). The calculated TM5 burdens are representative of the whole vertical domain of the atmosphere, including the stratosphere. The NOAA method gradients are compared with TM5 burden gradients to assess the representativeness of the MBL measurements using the NOAA method.

A full 3-D inversion of these measurements using an atmospheric transport model accounts for the transport and sampling effect (within the uncertainty of the transport model). To investigate whether the transport and sampling adjustments improve the consistency with inverse modeling results, we made use of globally inverted CH_4 fluxes made available by the Copernicus Atmospheric Monitoring Service. For this study, release "v16r2" was used covering the period 1990–2016 using NOAA surface observations for the inversion (Segers & Houweling, 2018). The inversion method uses a four-dimensional variational data assimilation (4-D VAR)optimization technique with the TM5 model, following a configuration similar to Bergamaschi et al. (2013). In a similar way to this study, their model is driven by ECMWF ERA-Interim meteorological data including convective fluxes. The analysis using these data concentrates on the transport and sampling adjustments to the IHD and IPD.

3. Results

3.1. Global Annual CH_4 Increases

First, we analyze the TM5-derived annual increase, comparing the annual atmospheric increase over the full vertical domain with the increase derived using the NOAA method (see Figure 1a). As expected, the full domain's burden shows only small year-to-year variability ($1\sigma = 0.24$ ppb/year). These small variations are caused by variations in the atmospheric sink due to changes in the spatial correlation between the global CH_4 mass distribution and the location of the sink, as modified by transport (see Warwick et al., 2002). This effect has a rather small influence on the calculated CH_4 annual increase. If the annual increase variations are derived using the NOAA method applied to TM5-sampled station output, the variability is significantly larger ($1\sigma = 1.09$ ppb/year). The difference between the two annual increase curves, which represents the error caused by sparse sampling in combination with transport, has a 1σ variation of 1.11 ppb/year. It quantifies the transport and sampling error of the NOAA method to infer the global annual CH_4 increase. A 1.11-ppb/year mean CH_4 increase is equal to 3.06-$TgCH_4$/year mass increase as per 2.76-$TgCH_4$/ppb conversion rate (Lassey et al., 2000). The annual increases determined with the NOAA method vary in the range of −2 to 2 ppb/year, which is similar to the range reported by Warwick et al. (2002).

In Figure 1b, we compare annual increases derived from TM5-sampled NOAA stations, using constant emissions and sinks in TM5, and the actual NOAA measurements, both using the NOAA method. As expected, the measurements show a larger variability ($1\sigma = 4.2$ ppb/year) as they are influenced not only by transport but also by changes in CH_4 sources and sinks. The correlation (R^2) between NOAA and TM5-derived annual increases is 0.11, indicating that 11% of the annual increase variation in the combined MBL measurements is explained purely by transport variability. Note that this assumes that TM5 represents the transport of CH_4 to the NOAA stations perfectly, which it likely does not. After subtracting the TM5-derived transport component from the measurement annual increases, the variability is reduced to 3.9 ppb/year (1σ). Such a reduction is expected when atmospheric transport contributes to the measured annual increase variation. Nevertheless, we conclude that the NOAA method provides a fairly accurate representation of variations in the annual global increase.

Next, we compare specific temporal signals observed in the measurements to those in the model driven by transport variations only. For example, the rise in the measurement's annual increases between 2013 and 2014 is 6.0 ppb/year^2 (5.5 ppb/year and 11.5 ppb/year annual increases from 2013 and 2014, respectively). In the model, the rise between 2013 and 2014 due to transport is already 3.6 ppb/year^2 (−1.7 ppb/year in 2013 to +1.9 ppb/year in 2014) explaining as much as 60% of the rise. After subtracting the transport and sampling effect (olive curve in Figure 1b), the rise from 2013 to 2014 (2.4 ppb/year^2) becomes comparable to the

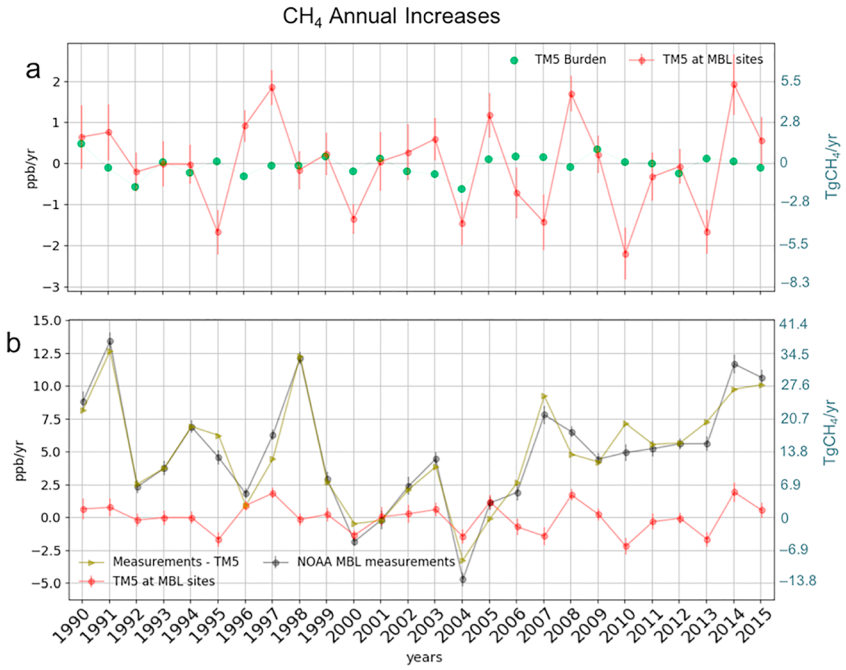

Figure 1. Annual global increases of CH_4 and the influence of transport and sampling effect, in parts per billion per year on left hand *y* axis and in teragrams CH_4 year on right hand *y* axis (conversion factor = 2.76 $TgCH_4$/ppb as per Lassey et al., 2000). (a, b) The red curve is derived from TM5 using the NOAA method. Error bars represent the 1σ uncertainties of annual increases reported by NOAA, using the method of Dlugokencky et al. (1994). Panel (a) Green line: increases inferred from TM5 calculated atmospheric burdens. Panel (b) Black line: increases inferred from NOAA measurements using the NOAA method; olive: difference with TM5 (red line, identical to [a]). NOAA = National Oceanic and Atmospheric Administration; MBL = marine boundary layer.

year before (1.6 ppb/year^2). Also, with the same adjustment, the annual increase during 2015, an El Niño year with annual increase of 10 ppb/year, becomes larger than the annual increase during 2014 (= 9.7 ppb/year).

3.2. Zonal Growth Rates

The latitudinal variation in the zonal growth rate of mean CH_4 is shown in Figure 2. All numbers in this figure are derived using the NOAA method, applied to measurements (Figure 2a) and TM5 output (Figure 2b).

Zonal growth rate from the measurements are mostly positive except for 1999 to 2006, when the global growth in atmospheric CH_4 was close to zero, and immediately after the eruption of Mount Pinatubo in 1991. The 1σ variability of the zonal growth rate in Figure 2a is 5.6 ppb/year, with values ranging from −15 to 22 ppb/year. The corresponding variability in the TM5-derived transport contribution is 3.8 ppb/year, ranging from −18 to 13 ppb/year. The correlation coefficient (R^2) between the measurements and TM5 is 0.19, as shown in Figures 2a and 2b. It means that for zonal averages, the fraction of variability explained by transport (= 19%) is higher than for the annual global increases (=11%). The difference between the atmospheric measurements and the TM5-derived contribution of transport and sampling is shown in Figure 2c. After accounting for transport and sampling, the 1σ variability is reduced to 5.0 ppb/year (with range = −10 to 21 ppb/year), consistent, like before, with the TM5-simulated transport accounting for a fraction of the observed variability.

The variability due to transport and sampling is larger in the Northern Hemisphere (1σ = 4.6 ppb/year) than in the Southern Hemisphere (1σ = 2.5 ppb/year). This is likely due to larger CH_4 emissions, and hence larger mixing ratio gradients, in the Northern Hemisphere. This difference between hemispheric growth rate variabilities is also present in the measurements, although less pronounced than in the transport component: 1σ of 6.0 ppb/year and 5.1 ppb/year in the Northern and Southern Hemisphere, respectively. Correlations between measured zonal growth rates and corresponding contributions from transport and sampling amount to r^2 = 0.20 in the Northern Hemisphere, and r^2 = 0.16 in the Southern Hemisphere, confirming the larger contribution from transport and sampling to the zonal growth rate in the Northern Hemisphere.

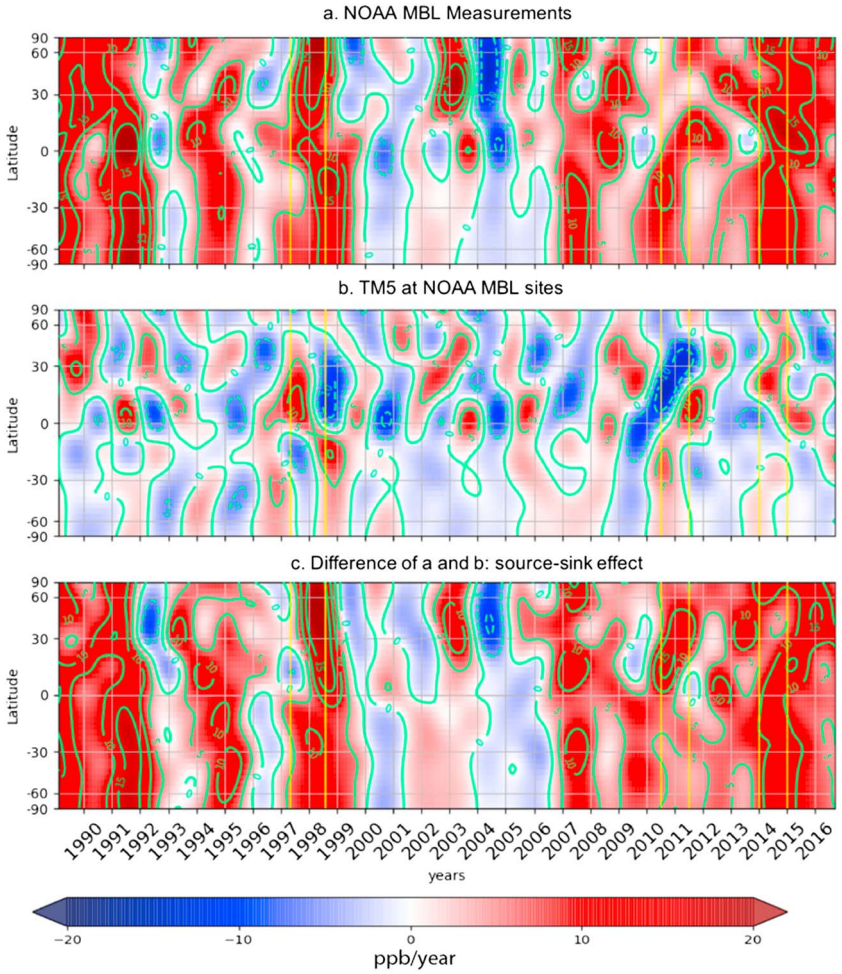

Figure 2. The latitudinal dependence of the CH_4 growth rate (referred as zonal growth rates in the main) derived using (a) the NOAA method applied to MBL measurements, (b) the TM5 transport-only simulation, and (c) the difference of (a) minus (b). Red colors indicate positive growth rates; blue colors represent negative growth rates. The green numbered growth rate contours are in ppb/year. The yellow vertical lines mark the beginning and end of three periods discussed in the main text: (i) El Niño of 1998, (ii) La Niña of 2010, and (iii) 2014. NOAA = National Oceanic and Atmospheric Administration; MBL = marine boundary layer.

Particularly interesting growth rate anomalies in Figure 2 are discussed here:

1. A growth rate of 15 ppb/year in the northern tropics during 2014, suggesting that this region played a leading role in the abrupt global CH_4 increase during 2014. However, according to Figure 2b this zonal anomaly can be explained largely by transport, as found in our global analysis already. After accounting for the transport sampling influence, the 2014 CH_4 growth actually appears to originate more from the Southern Hemisphere. This is consistent with the hypothesis of Nisbet et al. (2016) that emissions in the Southern Tropics were enhanced during 2014 as it was an exceptionally warm and wet year in Southern Africa and Amazonia.
2. The La Niña of 2011 led to a significant redistribution of CH_4 between the hemispheres driven by changes in transport, as shown in Figure 2b for 2011. In this year, inter-hemispheric transport was strengthened, which would imply a negative apparent growth rate anomaly in the Northern Hemisphere. However, this influence is not visible in the CH_4 measurements, suggesting a compensating influence by an emission increase in the Northern Hemisphere. This finding is consistent with increased wetland emissions in the Northern Tropics reported by Pandey et al. (2017). After accounting for transport and sampling, this event shows up as a 15 ppb/year growth rate anomaly in the Northern Tropics in Figure 2c.

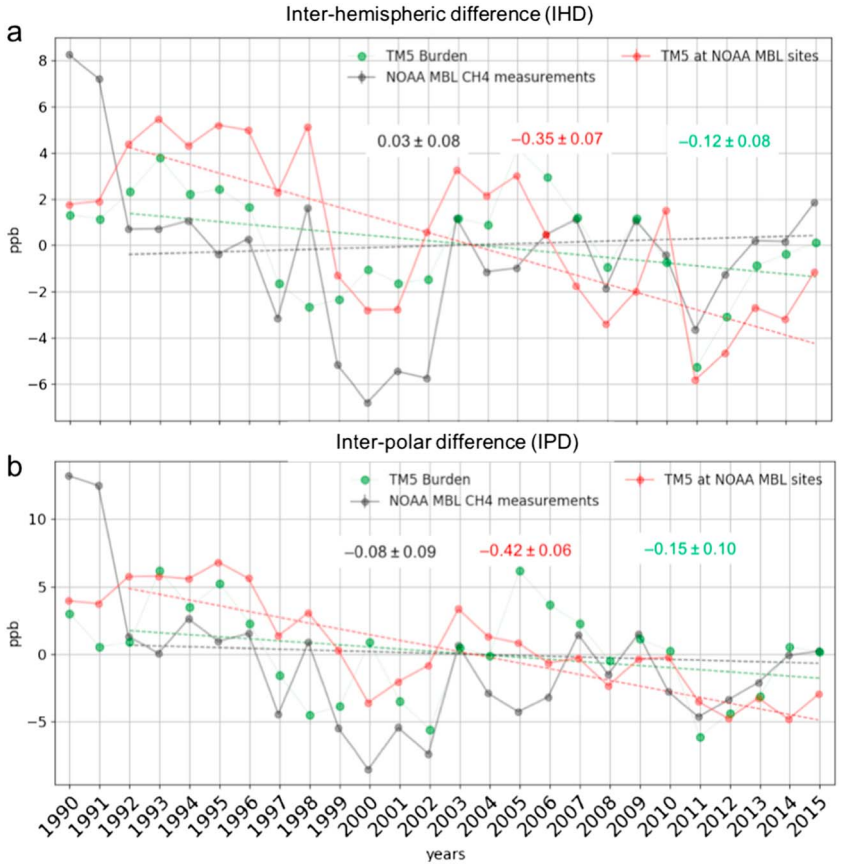

Figure 3. The interannual variability of the (a) inter-hemispheric and (b) inter-polar difference of CH_4. The straight dashed lines are the mean trend lines of each curve for 1992 to 2015 in the corresponding colors, and the numbers quantify the slope of trend lines. NOAA = National Oceanic and Atmospheric Administration; MBL = marine boundary layer.

3. The El Niño of 1998 caused a large increase in the global CH_4 growth rate (~12 ppb/year, see Figure 1b). The measurements show increased growth rates in both hemispheres. However, accounting for transport, the strongest increase was in the Northern Hemisphere.

3.3. Spatial Gradients

Next, we focus on the interannual variability of spatial gradients of CH_4: the inter-polar difference (IPD) and the inter-hemispheric difference (IHD). These gradients provide information about emission differences between the hemispheres.

The interannual variability of IHD is plotted in Figure 3a. The IHD of CH_4 measurements has an insignificant trend of 0.03 ± 0.08 ppb/year between 1992 and 2015. The TM5-derived influence of atmospheric transport on the IHD is -0.35 ± 0.07 ppb/year using the NOAA method and -0.12 ± 0.08 ppb/year using hemispheric burdens. These results point to an acceleration of inter-hemispheric transport (Krol et al., 2018; Naus et al., 2019; Patra et al., 2011). After adjusting the measurements for transport influences, we obtain a positive trend of $+0.37 \pm 0.06$ ppb/year (see Figure 4a), which indicates that the CH_4 emissions in the Northern Hemisphere are increasing faster than in the Southern Hemisphere.

The interannual variability of IPD is plotted in Figure 3b. It shows time variations that are qualitatively similar to IHD, except for a larger drop between 1991 and 1992. The ~10 ppb drop in IPD from 1991 to 1992 has been attributed to the collapse of fossil fuel production in Russia following the breakup of the Soviet Union in 1991 (Dlugokencky et al., 2011). Excluding this event, the trend in the measured IPD time series (1992–2015) is -0.08 ± 0.09 ppb/year (black dashed line). However, atmospheric transport contributed -0.15 ± 0.10 ppb/year (green dashed line), as derived from TM5 burdens. Sampling TM5 at NOAA MBL

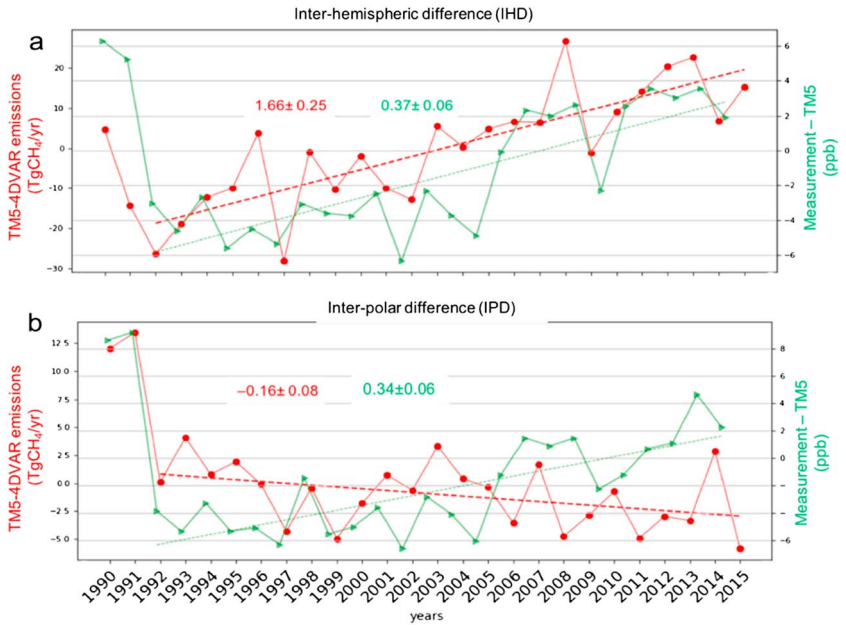

Figure 4. (a, b) Interannual variability of the spatial gradients of CH_4 in measurements, after removing transport and sampling effect, using the *National Oceanic and Atmospheric Administration method* (green line, right-hand *y* axis) and in optimized CH_4 emissions of TM5-4-D VAR inversions (red line, left-hand *y* axis). The straight dashed lines are the mean trend lines, with trend values written in the corresponding colors. 4-D VAR = four-dimensional variational data assimilation.

sites amplifies the IPD trend to -0.42 ± 0.06 ppb/year (red dashed line). After adjusting for transport, that is, taking the difference between the black and red lines in Figure 3b, we find a positive trend of 0.34 ± 0.06 ppb/year in the resulting time series (Figure 4b). This analysis shows that trends in the spatial gradients due to changing source and sinks are masked by trends due to transport and sampling.

To investigate whether the transport and sampling adjustments improve the consistency with inverse modeling results, we made use of global CH_4 fluxes made available by the Copernicus Atmospheric Monitoring Service. We find that the transport and sampling adjusted trend in IHD of $+0.37 \pm 0.06$ ppb/year agrees with an increasing difference between the emissions of Northern Hemisphere and Southern Hemisphere of 1.7 $TgCH_4/year^2$ (see Figure 4a). However, this is not the case for the IPD (see Figure 4b), where we find a small negative trend in the IPD of the emissions, that is, the difference between emissions in northern polar regions and southern polar regions, of -0.16 ± 0.08 $TgCH_4/year^2$. This is contrary to the positive trend of 0.34 ± 0.06 ppb/year found in transport-adjusted measurement IPD. The IPD trend of the optimized emissions agrees with Sweeney et al. (2016), who found, contrary to expectations, no observable increase in Arctic CH_4 emissions despite a 1.2 ± 0.8 °C/decade temperature increase in the region. The most likely explanation for the positive IPD measurements trend is a fast increase in midlatitude emissions combined with rapid intrahemispheric transport. This finding agrees with Dimdore-Miles et al. (2018), who showed that the IPD metric has difficulty in differentiating between Arctic and other northern hemispheric emissions.

4. Discussion and Conclusions

The atmospheric transport of CH_4 has been simulated in the tracer transport model TM5 using annually repeating sources and sinks, but varying meteorology, to investigate the influence of atmospheric transport on the CH_4 spatiotemporal gradients that are inferred from the MBL measurements of global monitoring networks. We demonstrate that atmospheric transport, in combination with the limited sampling density of atmospheric measurement networks, gives rise to variations in the CH_4 gradients, which are not caused by source or sink changes.

We find that in the global atmosphere, transport variations largely cancel out, as demonstrated by the low variability of the global burden in the TM5 transport-only simulation ($1\sigma = 0.24$ ppb/year), which originates from differences in the colocation of the CH_4 and oxidant fields. It means that the influence of transport

arises from incomplete global sampling by the MBL measurement. Such influences are unavoidable and acceptable as long as they are properly accounted for when making inferences from the data.

For assessing the annual global CH_4 increases, a measurement-only approach using existing background MBL sites is fairly accurate (1σ error = 1.11 ppb/year, with values ranging between −2 and 2 ppb/year for specific years). However, extending a measurement-only analysis to hemispheric or latitudinal variations is more problematic as transport influences quickly become significant or even dominant. The impact of transport on zonal growth rate variations derived from the data has 1σ variability of 3.8 ppb/year. The latitudinal distribution of zonal growth rate anomalies during strong El Niño and La Niña events is significantly impacted by concomitant changes in inter-hemispheric transport and can therefore not be attributed to the origin of anomalous sources and sinks without taking transport influences into account.

We find a large impact of transport and sampling effect on the inter-hemispheric and inter-polar difference (IHD and IPD). The positive trend of 0.37 ± 0.06 ppb/year in IHD, found after adjusting for transport and sampling, is likely caused by an increase in northern midlatitude emissions. We also find that the transport adjusted trend in IPD of 0.34 ± 0.06 ppb/year is not driven by increased emissions in the Arctic but is influenced by intrahemispheric transport from midlatitudes. Because of this, we infer that IPD might not be a reliable metric of trends in Arctic emissions.

Our findings are relevant not only for growth rate metrics based only on measurements from the global networks but also for the use of box models to investigate the origin of observed growth rate anomalies on relatively short time scales (within a few years). While it is true that the impacts of transport and sampling effect will reduce when analyzing multiyear averages, trends in atmospheric dynamics play a role as well, as shown here for the IHD, which require careful consideration when using box models. The implications of transport and sampling effect are particularly relevant for two-box model studies that use the observed inter-hemispheric difference to infer trends in hemispheric sources and sinks. Naus et al. (2019) analyze the implication of ignoring transport and sampling effect in such studies in detail.

A rapidly expanding archive of total column retrievals of CH_4 (XCH_4) is available from SCIAMACHY, GOSAT, and recently also S5p TROPOMI, covering roughly the past 1.5 decade. Satellites have the advantage over surface measurements that they are sensitive to most of the vertical column of the atmosphere, especially for sensors measuring in the Short-Wave InfraRed (see Jacob et al., 2016). In addition, satellites provide better spatial coverage than surface networks. However, satellite retrievals are more susceptible to systematic and regionally varying biases than calibrated surface measurements, making it difficult to take advantage of the favorable sampling. Further regional trends in satellite measurement are also affected by transport and sampling effect as shown by Bruhwiler et al. (2017). The representativeness of satellite retrievals, given their characteristic limitations in spatiotemporal coverage due to cloudiness, availability of sunlight, and so forth, would be worth assessing in the same fashion as we have done in this study for the surface network.

On a final note, we like to stress that CH_4 measurements from global surface networks like NOAA remain an indispensable source of information for monitoring the CH_4 budget and its variability in the atmosphere and for calibrating models and satellite data. However, results presented in this paper show that transport and sampling effect should be considered when linking measurement gradients to changes in sources and sinks, particularly at regional scales.

Acknowledgments
We acknowledge the support by the Netherlands Organization for Scientific Research (NWO) and Copernicus Atmosphere Monitoring Service ("CAMS_73 Greenhouse gases fluxes"). The TM5 model computations were carried out on the Dutch national supercomputer Cartesius maintained by SURFSara (www.surfsara.nl). NOAA CH_4 measurements are freely available from NOAA's public ftp server (ftp://aftp.cmdl.noaa.gov/data).

References

Bergamaschi, P., Houweling, S., Segers, A., Krol, M., Frankenberg, C., Scheepmaker, R. A., et al. (2013). Atmospheric CH_4 in the first decade of the 21st century: Inverse modeling analysis using SCIAMACHY satellite retrievals and NOAA surface measurements. *Journal of Geophysical Research: Atmospheres*, *118*, 7350–7369. https://doi.org/10.1002/jgrd.50480

Bruhwiler, L. M., Basu, S., Bergamaschi, P., Bousquet, P., Dlugokencky, E., Houweling, S., et al. (2017). U.S. CH_4 emissions from oil and gas production: Have recent large increases been detected? *Journal of Geophysical Research: Atmospheres*, *122*, 4070–4083. https://doi.org/10.1002/2016JD026157

Chen, Y. H., & Prinn, R. G. (2005). Atmospheric modeling of high- and low-frequency methane observations: Importance of interannually varying transport. *Journal of Geophysical Research*, *110*, D10303. https://doi.org/10.1029/2004JD005542

Dee, D. P., Uppala, S. M., Simmons, A. J., Berrisford, P., Poli, P., Kobayashi, S., et al. (2011). The ERA-Interim reanalysis: Configuration and performance of the data assimilation system. *Quarterly Journal of the Royal Meteorological Society*, *137*(656), 553–597. https://doi.org/10.1002/qj.828

Dimdore-Miles, O. B., Palmer, P. I., & Bruhwiler, L. P. (2018). Detecting changes in Arctic methane emissions: Limitations of the inter-polar difference of atmospheric mole fractions. *Atmospheric Chemistry and Physics*, *18*(24), 17,895–17,907. https://doi.org/10.5194/acp-18-17895-2018

Dlugokencky, E., Nisbet, E., Fisher, R., & Lowry, D. (2011). Global atmospheric methane: Budget, changes and dangers. *Philosophical Transactions of the Royal Society*, *369*(1943), 2058–2072. https://doi.org/10.1098/rsta.2010.0341

Dlugokencky, E. J., Houweling, S., Bruhwiler, L., Masarie, K. A., Lang, P. M., Miller, J. B., & Tans, P. P. (2003). Atmospheric methane levels off: Temporary pause or a new steady-state? *Geophysical Research Letters*, *30*(19), 1992. https://doi.org/10.1029/2003GL018126

Dlugokencky, E. J., Lang, P. M., Crotwell, A. M., Mund, J. W., Crotwell, M. J., & Thoning, K. W. (2017). Atmospheric methane dry air mole fractions from the NOAA ESRL carbon cycle cooperative global air sampling network, 1983–2016, Version: 2017-07-28, Path: ftp://aftp.cmdl.noaa.gov/data/trace_gases/ch4/flask/surface/

Dlugokencky, E. J., Steele, L. P., Lang, P. M., & Masarie, K. A. (1994). The growth rate and distribution of atmospheric methane. *Journal of Geophysical Research*, *99*(D8), 17,021–17,043. https://doi.org/10.1029/94JD01245

Hausmann, P., Sussmann, R., & Smale, D. (2016). Contribution of oil and natural gas production to renewed increase in atmospheric methane (2007–2014): Top–down estimate from ethane and methane column observations. *Atmospheric Chemistry and Physics*, *16*(5), 3227–3244. https://doi.org/10.5194/acp-16-3227-2016

Houweling, S., Krol, M., Bergamaschi, P., Frankenberg, C., Dlugokencky, E. J., Morino, I., et al. (2014). A multi-year methane inversion using SCIAMACHY, accounting for systematic errors using TCCON measurements. *Atmospheric Chemistry and Physics*, *14*(8), 3991–4012. https://doi.org/10.5194/acp-14-3991-2014

Huijnen, V., Williams, J., van Weele, M., van Noije, T., Krol, M., Dentener, F., et al. (2010). The global chemistry transport model TM5: Description and evaluation of the tropospheric chemistry version 3.0. *Geoscientific Model Development*, *3*(2), 445–473. https://doi.org/10.5194/gmd-3-445-2010

Jacob, D. J., Turner, A. J., Maasakkers, J. D., Sheng, J., Sun, K., Liu, X., et al. (2016). Satellite observations of atmospheric methane and their value for quantifying methane emissions. *Atmospheric Chemistry and Physics*, *16*(22), 14,371–14,396. https://doi.org/10.5194/acp-16-14371-2016

Janssens-Maenhout, G., Crippa, M., Guizzardi, D., Muntean, M., Schaaf, E., Dentener, F., et al. (2017). EDGAR v4.3.2 Global Atlas of the three major Greenhouse Gas Emissions for the period 1970–2012, *Earth System Science Data Discussions*. https://doi.org/10.5194/essd-2017-79

Jöckel, P., Tost, H., Pozzer, A., Brühl, C., Buchholz, J., Ganzeveld, L., et al. (2006). The atmospheric chemistry general circulation model ECHAM5/MESSy1: Consistent simulation of ozone from the surface to the mesosphere. *Atmospheric Chemistry and Physics*, *6*(12), 5067–5104. https://doi.org/10.5194/acp-6-5067-2006

Kirschke, S., Bousquet, P., Ciais, P., Saunois, M., Canadell, J. G., Dlugokencky, E. J., et al. (2013). Three decades of global methane sources and sinks. *Nature Geoscience*, *6*(10), 813–823. https://doi.org/10.1038/ngeo1955

Krol, M., de Bruine, M., Killaars, L., Ouwersloot, H., Pozzer, A., Yin, Y., et al. (2018). Age of air as a diagnostic for transport timescales in global models, *Geoscientific Model Development*, *11*, 3109–3130. https://doi.org/10.5194/gmd-11-3109-2018

Krol, M., Houweling, S., Bregman, B., van den Broek, M., Segers, A., van Velthoven, P., et al. (2005). The two-way nested global chemistry-transport zoom model TM5: Algorithm and applications. *Atmospheric Chemistry and Physics*, *5*(2), 417–432. https://doi.org/10.5194/acp-5-417-2005

Lassey, K. R., Lowe, D. C., & Manning, M. R. (2000). The trend in atmospheric methane δ13C and implications for isotopic constraints on the global methane budget. *Global Biogeochemical Cycles*, *14*(1), 41–49. https://doi.org/10.1029/1999GB900094

Masarie, K. A., & Tans, P. P. (1995). Extension and integration of atmospheric carbon dioxide data into a globally consistent measurement record. *Journal of Geophysical Research*, *100*(D6), 11,593–11,610. https://doi.org/10.1029/95JD00859

Naus, S., Montzka, S. A., Pandey, S., Basu, S., Dlugokencky, E. J., & Krol, M. (2019). Constraints and biases in a tropospheric two-box model of OH. *Atmospheric Chemistry and Physics*, *19*(1), 407–424. https://doi.org/10.5194/acp-19-407-2019

Nisbet, E. G., Dlugokencky, E. J., & Bousquet, P. (2014). Methane on the Rise—Again. *Science*, *343*(6170), 493–495. https://doi.org/10.1126/science.1247828

Nisbet, E. G., Dlugokencky, E. J., Manning, M. R., Lowry, D., Fisher, R. E., France, J. L., et al. (2016). Rising atmospheric methane: 2007–2014 growth and isotopic shift. *Global Biogeochemical Cycles*, *30*, 1356–1370. https://doi.org/10.1002/2016GB005406

Pandey, S., Houweling, S., Krol, M., Aben, I., Monteil, G., Nechita-Banda, N., et al. (2017). Enhanced methane emissions from tropical wetlands during the 2011 La Niña. *Scientific Reports*, *7*(1), 1–8. https://doi.org/10.1038/srep45759

Patra, P. K., Houweling, S., Krol, M., Bousquet, P., Belikov, D., Bergmann, D., et al. (2011). TransCom model simulations of CH_4 and related species: Linking transport, surface flux and chemical loss with CH_4 variability in the troposphere and lower stratosphere. *Atmospheric Chemistry and Physics*, *11*(24), 12,813–12,837. https://doi.org/10.5194/acp-11-12813-2011

Rigby, M., Montzka, S. A., Prinn, R. G., White, J. W. C., Young, D., O'Doherty, S., et al. (2017). Role of atmospheric oxidation in recent methane growth. *Proceedings of the National Academy of Sciences of the United States of America*, *114*(21), 5373–5377. https://doi.org/10.1073/pnas.1616426114

Sapart, C. J., Monteil, G., Prokopiou, M., van de Wal, R. S. W., Kaplan, J. O., Sperlich, P., et al. (2012). Natural and anthropogenic variations in methane sources during the past two millennia. *Nature*, *490*(7418), 85–88. https://doi.org/10.1038/nature11461

Schaefer, H., Fletcher, S. E. M., Veidt, C., Lassey, K. R., Brailsford, G. W., Bromley, T. M., et al. (2016). A 21st-century shift from fossil-fuel to biogenic methane emissions indicated by $^{13}CH_4$. *Science*, *352*(6281), 80–84. https://doi.org/10.1126/science.aad2705

Schwietzke, S., Sherwood, O. A., Bruhwiler, L. M. P., Miller, J. B., Etiope, G., Dlugokencky, E. J., et al. (2016). Upward revision of global fossil fuel methane emissions based on isotope database. *Nature*, *538*(7623), 88–91. https://doi.org/10.1038/nature19797

Segers, A. J., & Houweling, S. (2018). Validation of the CH_4 surface flux inversion–reanalysis 1990–2016. Ref: CAMS73_2015SC2_D73.2.4.4-2016_201712_validation_CH4_2000-2016_v1.

Spahni, R., Wania, R., Neef, L., van Weele, M., Pison, I., Bousquet, P., et al. (2011). Constraining global methane emissions and uptake by ecosystems. *Biogeosciences*, *8*(6), 1643–1665, https://doi.org/10.5194/bg-8-1643-2011

Spivakovsky, C. M., Logan, J. A., Montzka, S. A., Balkanski, Y. J., Foreman-Fowler, M., Jones, D. B. A., et al. (2000). Three-dimensional climatological distribution of tropospheric OH: Update and evaluation. *Journal of Geophysical Research*, *105*(D7), 8931–8980. https://doi.org/10.1029/1999JD901006

Sweeney, C., Dlugokencky, E., Miller, C. E., Wofsy, S., Karion, A., Dinardo, S., et al. (2016). No significant increase in long-term CH_4 emissions on North Slope of Alaska despite significant increase in air temperature. *Geophysical Research Letters*, *43*, 6604–6611. https://doi.org/10.1002/2016GL069292

Thompson, R. L., Nisbet, E. G., Pisso, I., Stohl, A., Blake, D., Dlugokencky, E. J., et al. (2018). Variability in atmospheric methane from fossil fuel and microbial sources over the last three decades. *Geophysical Research Letters*, *45*, 11,499–11,508. https://doi.org/10.1029/2018GL078127

Turner, A. J., Frankenberg, C., Wennberg, P. O., & Jacob, D. J. (2017). Ambiguity in the causes for decadal trends in atmospheric methane and hydroxyl. *Proceedings of the National Academy of Sciences of the United States of America*, *114*(21), 5367–5372. https://doi.org/10.1073/pnas.1616020114

van der Laan-Luijkx, I. T., van der Velde, I. R., Krol, M. C., Gatti, L. V., Domingues, L. G., Correia, C. S. C., et al. (2015). Response of the Amazon carbon balance to the 2010 drought derived with Carbon Tracker South America. *Global Biogeochemical Cycle*, *29*, 1092–1108. https://doi.org/10.1002/2014GB005082

Warwick, N. J., Bekki, S., Law, K. S., Nisbet, E. G., & Pyle, J. A. (2002). The impact of meteorology on the interannual growth rate of atmospheric methane. *Geophysical Research Letters*, *29*(20), 1947. https://doi.org/10.1029/2002GL015282

Worden, J. R., Bloom, A. A., Pandey, S., Jiang, Z., Worden, H. M., Walker, T. W., et al. (2017). Reduced biomass burning emissions reconcile conflicting estimates of the post-2006 atmospheric methane budget. *Nature Communications*, *8*(1), 2227. https://doi.org/10.1038/s41467-017-02246-0